Periodic actin structures in neuronal axons are required to maintain microtubules

Yue Qu[1*], Ines Hahn[1*], Stephen Webb[2], Andreas Prokop[1†]

[1]Faculty of Life Sciences, Michael Smith Building, Oxford Road, Manchester M13 9PT, United Kingdom
[2]Science and Technology Facilities Council, Research Complex at Harwell, Rutherford Appleton Laboratory, Harwell Campus Didcot, OX11 0QX, UK
*These authors contributed equally to this work.
[†]To whom correspondence should be addressed. E-mail: Andreas.Prokop@manchester.ac.uk

Key words: *Drosophila*, neurodegeneration, axons, actin, cytoskeleton, microtubules

Abstract

Axons are cable-like neuronal processes wiring the nervous system. These delicate structures have to be sustained for an organism's lifetime. Their backbones and life-sustaining transport highways are formed by parallel microtubules bundles, surrounded by recently discovered periodic axonal actin structures (PAAS). Here we demonstrate the first functional role of PAAS. Via super-resolution microscopy we show that PAAS are evolutionarily conserved. Imaging of 11 genetic and 3 drug-based manipulations of actin or actin regulators revealed that these structures are composed of short actin filaments dependent on Adducin, Spectrin, Ena/VASP, Arp2/3 and DAAM. They are required to maintain axonal microtubules through sustained polymerisation, in parallel to independent stabilising mechanisms mediated by microtubule-binding spectraplakin proteins. Removing both stabilisation mechanisms triggers axon degeneration. Our data establish PAAS as functionally relevant, evolutionarily conserved structural components of axons. They provide new conceptual explanations for neural disorders linked to cortical actin regulators and for injury-derived axon degeneration.

Results

Axons are the slender cable-like extensions of neurons, up to meter-long, which wire the nervous system and propagate nerve impulses (PROKOP 2013). Accordingly, their damage causes impairment of movement or cognitive deficits (SMITH *et al.* 2000). Their delicate structure often has to be maintained for an organism's lifetime. Unsurprisingly, we gradually lose half our axons during healthy ageing and far more in neurodegenerative diseases (ADALBERT and COLEMAN 2012).

We want to understand the mechanisms of long-term axon maintenance, which will also be relevant for our understanding of axon pathology during ageing and disease. For this, we focus on the parallel bundles of microtubules (MTs) running along axons to form their structural backbones and highways for live-sustaining transport (PROKOP 2013). Here we use the experimentally amenable neurons of the fruit fly *Drosophila* to demonstrate that the stabilisation and maintenance of axonal MT bundles requires axonal actin.

Periodic axonal actin structures are evolutionarily conserved in *Drosophila* neurons

Axons of mammalian neurons display periodic axonal actin structures (PAAS) where F-actin is bundled into rings which are evenly spaced by ~180 nm intervals. PAAS were proposed, predominantly from imaging data, to represent cortical F-actin consisting of short, Adducin-

capped filaments cross-linked by Spectrins (D'ESTE *et al.* 2015; GANGULY *et al.* 2015; LUKINAVIČIUS *et al.* 2014; XU *et al.* 2013; ZHONG *et al.* 2014).

We studied cultured primary neurons of the fruit fly *Drosophila* at >6DIV (days *in vitro*) using structured illumination microscopy (SIM). In their axons, we found occasional longitudinal actin trails (Fig.S1A; also described for mammalian neurons) (GANGULY *et al.* 2015) and highly abundant periodic actin pattern with a repeat length of ~184nm, clearly representing PAAS (Figs.1A,B,E,S1). We validated our findings using stimulated emission depletion (STED) microscopy (Fig.1C,D) and control experiments with SIM (Figs.1A,S1B). The abundance of PAAS (amount of axon sections displaying PAAS; see Methods) gradually increased from 20% at 6HIV (hours *in vitro*) to 82% at 10DIV (Fig.1F), similar to developmental delay observed in mammalian neurons (D'ESTE *et al.* 2015; XU *et al.* 2013).

Functional proof that PAAS represent cortical F-actin networks

We next capitalised on the robust SIM readout combined with the experimental and genetic amenability of *Drosophila* neurons, to study the effects of mutations in 11 different actin regulators and treatment with 3 actin-affecting drugs on PAAS abundance in neurons at 10DIV.

Treatment with the actin de-polymerising drug cytochalasinD (CytoD; 4hrs @800nM) significantly reduced normalised PAAS abundance to 32%. In contrast, treatment with the actin de-polymerising drug LatrunculinA (LatA; 4hrs @200nM) caused only a non-significant reduction to 94% (Fig.2A''',E',F). When applying these same drug treatments to younger neurons, they efficiently eliminated filopodial cell protrusions, which provide effective readouts for long, dynamic actin filaments (Fig.S2) (GONÇALVES-PIMENTEL *et al.* 2011). Therefore, long actin filaments are more vulnerable than PAAS, as similarly reported for mammalian neurons (XU *et al.* 2013). They do not resist treatment with CytoD (actively destabilising barbed filament ends) (PETERSON and MITCHISON 2002) but to LatA (mainly suppressing polymerisation by sequestering actin monomers) (PETERSON and MITCHISON 2002).

PAAS resistance to LatA treatment may be explained by filament stabilisation through Adducin-Spectrin (BAINES 2010), both known to be present in mammalian PAAS (XU *et al.* 2013). As predicted, null mutant alleles of Adducin (*hts*^{1} mutant neurons) and ß-Spectrin (*β-Spec*^{S012}) drastically reduced the relative PAAS abundance to 33% and 58% (Fig.2C',D',F), analogous to effects caused by βII-Spectrin depletion in mammalian neurons (ZHONG *et al.* 2014). In contrast, the same *hts*^{1} and *β-Spec*^{S012} mutant alleles caused no reduction in filopodial length in young neurons (maternal contribution removed; Fig.S2), further indicating that actin networks of PAAS are different. In contrast, only non- or mildly significant PAAS reductions were observed upon loss of other typical components of cortical actin (BAINES 2010) including α-Spectrin (forms hetero-oligomers with ß-spectrin but lacks actin and Adducin binding sites; *α-Spec*^{rg41}: 89%) and Ankyrin2 (links cortical actin to the membrane and other structures; *ank2*^{518}: 92%; Fig.2F). Analogously, AnkyrinB depletion in mouse neurons had little effect on PAAS (ZHONG *et al.* 2014).

Actin filaments in PAAS were proposed to be short (XU *et al.* 2013) and should therefore be little dependent on elongation factors. Accordingly, depletion of the actin elongation factor Profilin (*chic*^{221} allele; strongly affecting filopodial length; Fig.S2) (GONÇALVES-PIMENTEL *et al.* 2011) caused no significant reduction in PAAS abundance at 10DIV (Fig.2A'',F). In contrast, depletion of Ena/VASP (*ena*^{23} allele), a protein known to closely collaborate with Profilin in actin filament elongation (BEAR and GERTLER 2009; GONÇALVES-PIMENTEL *et al.* 2011),

significantly reduced PAAS abundance at 10DIV to 83% (Fig.2F). This could be explained through roles of Ena/VASP (but not Profilin) in the formation of new actin filaments (nucleation) (GONÇALVES-PIMENTEL *et al.* 2011), and nucleation should be particularly important for PAAS where actin filaments are short, hence high in number.

To test this, we depleted two distinct nucleators expressed in these neurons, Arp2/3 and the formin DAAM (GONÇALVES-PIMENTEL *et al.* 2011). Genetic depletion of three components required for Arp2/3 function (see Methods) showed a consistent reduction to ~80% (Fig.2F; *Arpc1*^{1}: 79%; *SCAR*$^{\Delta 37}$: 85%; *Hem*^{03335}: 75%). Neurons carrying the *DAAM*^{Ex68} null mutation or treated with the formin-inhibiting drug SMIFH2 (4hrs @10µM), showed an even stronger reduction to 60% and 68% (Fig.2B',F).

Therefore, PAAS are an evolutionary conserved articulation of cortical actin consisting of short and numerous filaments stabilised by Adducin-ß-Spectrin.

F-actin has MT-maintaining roles in axons

We next used the various manipulations from above to identify and study potential roles of PAAS. Important hints came from observations that CytoD-treated neurons showed frequent gaps in the tubulin staining along axons (DMSO, 5% of neurons; 800nM CytoD, 31%; 1.6µM CytoD, 83%; Fig.3A–C,E) or even complete loss of axons (DMSO: 24% of neurons, 800nM CytoD: 31% of neurons; 1.6µM CytoD: 45%; Fig.3D,F). These data indicated potential loss of axonal MTs in a dose-dependent manner and suggested that F-actin has MT-maintaining roles in axons.

To test this notion, we treated neurons for 2.5hrs (5.5-8HIV @20µM) with the microtubule-destabilising drug nocodazole which alone hardly affected axons (Fig.3E,F) (ALVES-SILVA *et al.* 2012; SÁNCHEZ-SORIANO *et al.* 2009). However, when this treatment was combined with 800nM CytoD (4-8HIV), values almost doubled compared to single CytoD treatment (axonal gaps: 60% of neurons; axon loss: 51%; Fig.3D–F). The same trend was observed when affecting MTs genetically by removing MT-binding spectraplakin proteins known to stabilise MTs against nocodazole (ALVES-SILVA *et al.* 2012; YANG *et al.* 1999). Neurons lacking the *Drosophila* spectraplakin Short stop (Shot; *shot*$^{3/sf20}$ allele) display normal abundance of PAAS when analysed with SIM (Fig.2F), suggesting that MT-maintaining roles of actin are in place. Accordingly, CytoD treatment (4-8HIV @800nM) almost doubled their axon loss from 36% to 64% (Fig.3F). In conclusion, MT maintaining roles of F-actin become particularly apparent when weakening MT networks via nocodazole application or removal of Shot.

Analyses of axonal gaps and axon loss are rather crude readouts for MT abundance, but *shot* mutant neurons provided us with an alternative mode of MT quantification. Their axons robustly display areas of MTs disorganisation where MTs are less coalescent and can often be seen as individual structures heavily criss-crossing each other (consequence of loosing normal functions of Shot in MT guidance and stabilisation; Fig.4A) (ALVES-SILVA *et al.* 2012; SÁNCHEZ-SORIANO *et al.* 2009). We predicted that loss of MTs involved in regions of disorganisation should result in a decreased area of disorganisation, which can be quantified as MT disorganisation index (MDI). If PAAS maintain MTs, their removal should strongly reduce the MDI. In agreement with this prediction, we found that the very high MDI of DMSO-treated *shot*^{3} mutant neurons at 8HIV (Tab.S4) was reduced to 0 upon CytoD treatment (4hrs @800nM; Fig.4G, H). For the following studies we used the MDI as the primary readout.

MT-stabilising properties correlate with the presence of PAAS

To test whether MT-stabilising roles of F-actin are mediated by PAAS, we systematically studied the effects of the different actin manipulations on MT maintenance in *shot* mutant neurons (using the MDI) and then correlated them with their effects on PAAS abundance. MDI measurements are easy to perform in young neurons (typically 6-8HIV), still possible at 3DIV and very difficult at 10DIV when axons can no longer be determined in their entire length within densely grown axon networks (Fig.S1). *Vice versa*, PAAS abundance is stable at 10DIV, but a far less reliable readout at 6-8HIV. To determine whether data can be correlated across developmental stages, we performed a few spot tests at 3DIV and 8HIV.

At 3DIV, *Drosophila* neurons have long undergone synaptic differentiation (occurs at 1DIV) (KÜPPERS-MUNTHER *et al.* 2004) and PAAS have reached ~50% abundance (Fig.1; Tab.S1). Our spot tests revealed that $shot^{3}$ mutant neurons displayed a high MDI at 3DIV (Fig.4I). When $shot^{3}$ was combined with manipulations known to affect PAAS abundance (4hr CytoD @800nM or double-mutant condition with $SCAR^{\Delta 37}$) the MDI was significantly reduced, whereas manipulations with little effect on PAAS (4hrs LatA @200nM or double-mutant condition with $chic^{221}$) showed no significant MDI reduction at 3DIV (Fig.4A,G,I). Therefore, four manipulations at 3DIV showed good correlation between the presence/absence of PAAS and the ability/inability to maintain axonal MTs.

At 8HIV, spot tests of neurons with SIM analyses revealed similar effects of actin manipulations on PAAS as were observed at 10DIV (Fig.2G). CytoD treatment (4hrs @800nM) or genetic loss of DAAM ($DAAM^{Ex68}$) or ß-Spectrin ($ß\text{-}Spectrin^{S012}$) reduced PAAS abundance significantly, whereas Profilin depletion ($chic^{221}$) had no effect. However, as similarly reported for mammalian neurons (ZHONG *et al.* 2014), young *Drosophila* neurons were more vulnerable to LatA treatment (4hrs LatA @200nM reduced PAAS abundance to 48%), suggesting a higher dependence on polymerisation during axon growth. To adapt for this condition, we reduced LatA application to 1hr, which no longer caused significant PAAS loss whilst still abolishing filopodia; Figs. 2G, S2G). Accordingly, 1hr LatA treatment caused no significant increase in axonal tubulin gaps or reduction in MDI, whereas 4hrs application significantly increased gaps to 19%, axon loss to 41% and reduced MDI to 22% (Figs.3E,F and 4I). We concluded that there is a quantitative but not a qualitative difference between young and old neurons.

Having convinced ourselves that the manipulations used cause comparable effects at different developmental stages, we combined further actin manipulations with functional deficiency of Shot. In these neurons, we assessed the MDI as a measure of the ability/inability to maintain MTs (Fig.4) and then correlated those data with PAAS abundance in wildtype neurons at 8HIV and 10DIV (Fig.2). We obtained a highly significant correlation between the presence/absence of PAAS and high/low values for MDI (Spearman correlation coefficient = 0.7821429, p = 0.0009016; Figs.5A, S3 and Tab.S1,S4) and concluded that PAAS essentially contribute to MT maintenance in axons.

Cortical F-actin promotes MT polymerisation

To validate our findings with another methodological approach and to study potential mechanisms involved in MT maintenance downstream of F-actin, we used live imaging analyses of $shot^{3}$ mutant neurons to study potential changes of MT behaviours upon acute drug application. As readout we used EB1::GFP which primarily localises as comets at plus ends of actively polymerising MTs (Mov.S1, Fig.6A,B) (ALVES-SILVA *et al.* 2012).

Upon application of CytoD to *shot*^{3} mutant neurons at either 6HIV or 3DIV, comets tended to change from steady propagation to stalling behaviour and then gradually fainted away; these effects were enhanced when increasing CytoD concentration from 800nM to 1.6µM (Fig.6C-E, Mov.S2). Detailed image analyses revealed a significant loss of comet numbers and significant slow-down of comet speed in *shot*^{3} mutant neurons at 6HIV and 3DIV (Fig.6C–E).

In contrast, wildtype neurons treated with CytoD at 6HIV or 3DIV showed no or very mild reductions in comet numbers (Fig.6C,D). However, at 6HIV the velocity of EB1 comets gradually decreased (Fig.6E). This probably causes reduced net plus MT polymerisation and could explain the gaps observed in axonal MT bundles of CytoD-treated wildtype neurons (Fig.3B,C). These effects of CytoD on comet behaviours are dose-dependent, paralleling dose-dependent effects on axonal gaps and axon loss (Figs.3E,F and 6C,E).

Application of LatA to wildtype and *shot*^{3} mutant neurons had no effect on comet number and velocity at 3DIV (Fig.6F–H). At 6HIV, we observed a drop in comet numbers and velocity only after an hour and only in *shot*^{3} mutant neurons (Fig.6F,H), consistent with our data for PAAS abundance, axonal gaps and MD when comparing 1hr and 4hrs LatA treatments (Figs.2G, 3E and 4H).

These data strongly support our hypothesis that PAAS play an important role in axonal MT maintenance, complementary to independent stabilisation through Shot. They indicate promotion of MT polymerisation as the likely cellular mechanism through which PAAS maintain MTs.

Discussion

Newly discovered roles for actin in the axonal shaft provide new opportunities

Here we demonstrate that PAAS are an evolutionarily conserved feature of axons, we provide functional proof of their nature as cortical actin networks and demonstrate an important role in MT maintenance, which we show to act in parallel to spectraplakin-dependent mechanisms of MT stabilisation. Our work has numerous implications for the understanding of axon biology in the context of development, maintenance, degeneration and regeneration, and it provides exciting new opportunities for the study of cortical actin beyond erythrocytes as the current prime model for such work.

New conceptual understanding of axon biology and disease

Parallel bundles of MTs are the essential backbones and transport highways of axons, and their maintenance is pivotal for axon longevity (ADALBERT and COLEMAN 2012; PROKOP 2013; PROKOP *et al.* 2013). MT-maintaining roles of PAAS offer therefore new conceptual explanations and investigative directions for brain disorders which have been linked to gene mutations of cortical actin regulators: cerebral palsy linked to human Adducin (ADD3) (KRUER *et al.* 2013), spinocerebellar ataxia to ß-spectrin (SPTBN2; OMIM ID: 600224, 615386), mental retardation to Ankyrin (ANK3; OMIM ID: 615493), or Baraitser-Winter syndrome and dystonia with neurodegenerative traits to actin itself (ACTB7; OMIM ID: 243310, 607371). In further support of our interpretation, β-Spectrin mutant neurons were shown to display axon breakage in *C. elegans* (HAMMARLUND *et al.* 2007) and axonal transport defects coupled to neurodegeneration in *Drosophila* (LORENZO *et al.* 2010).

Our results also provide important explanations for axon stump degeneration after injury, which is the initial step towards axon regeneration (BRADKE *et al.* 2012). Axon injury triggers

an elevation of intracellular free calcium levels leading to Calpain-mediated removal of actin-Spectrin. Interestingly, binding of calcium to EF-hand motifs of spectraplakins was reported to trigger their detachment from MTs (KA *et al.* 2014; KAPUR *et al.* 2012; WU *et al.* 2011). Therefore, calcium can remove both MT-stabilising mechanisms uncovered by our work. The significantly enhanced axon loss which we observed in experiments where both mechanisms were simultaneously eliminated (Fig.3F), may fundamentally mimic injury-induced axon retraction and provide new strategies for its study.

Here we pinpoint MT polymerisation as a process promoted through axonal actin which might also explain earlier reports that axons fail to form and elongate when actin is severely depleted (in DAAM and Arp2/3 double-deficient neurons) (GONÇALVES-PIMENTEL *et al.* 2011). However, PAAS are likely to play further roles in axons. Firstly, PAAS may be used by spectraplakins to guide polymerising MTs into ordered parallel bundles, a mechanism providing explanations for type IV hereditary sensory and autonomic neuropathy (OMIM ID: 614653) (ALVES-SILVA *et al.* 2012; PROKOP *et al.* 2013; SÁNCHEZ-SORIANO *et al.* 2009). Furthermore, cortical actin was proposed to contribute to Dynein/Dynactin mediated sliding of MTs and transport of MT fragments (MYERS *et al.* 2006), the spatial arrangements of transmembrane proteins along axons (relevant for action potentials or the adhesion to ensheathing glia) (BAINES 2010; MACHNICKA *et al.* 2014; ZHANG *et al.* 2016), and it may even contribute to the regulation of collateral branching (KALIL and DENT 2014). All these functions can now be studied with the tools and strategies established here.

A new cell model for the study of cortical actin

So far, erythrocytes have been the prime cellular model for the study of cortical F-actin (BAINES 2010). PAAS have now joined ranks providing a second biological context which can be investigated using the characteristic periodic actin pattern and MT network integrity as relevant readouts (GANGULY *et al.* 2015; LUKINAVIČIUS *et al.* 2014; XU *et al.* 2013; ZHONG *et al.* 2014). It remains to be seen whether the periodicity is an essential functional feature of these actin networks (as proposed for the spacing of ion channels) (ZHANG *et al.* 2016) or whether the mere presence of cortical actin is functionally sufficient. We observed strong functional contributions at 6HIV when PAAS abundance is low, yet cortical actin is likely to be present in less structured forms. The periodic arrangement of PAAS may simply be a secondary consequence of axon morphology where oscillations in one axis (i.e. along the axonal tube) could shuffle diffusely cross-linked cortical actin networks into linear, periodic patterns (HANNEZO *et al.* 2015).

Beside PAAS there are other actin structures in axon shafts including dense networks at the axon initial segment (selective filters for axonal transport) (GALIANO *et al.* 2012; LI *et al.* 2011; RASBAND 2010; WATANABE *et al.* 2012), shaft filopodia (considered important for collateral branching) (KALIL and DENT 2014), lamellipodial-like actin waves migrating along axon shafts (FLYNN *et al.* 2009), as well as transiently occurring longitudinal actin filaments (regulating synapse dynamics) (D'ESTE *et al.* 2015; GANGULY *et al.* 2015). All of those actin structures are likely to contain long dynamic actin filaments, and our correlative studies with a wide range of actin regulators would therefore suggest that they play no or only minor roles during MT maintenance.

Methods

Fly stocks

All mutant alleles used in this study are well characterised. The following embryonic lethal, loss-of-function mutant alleles were used:
The *Hu li tai shao*/adducin loss-of-function mutant allele ***hts*^{1}** is a strong hypomorphic allele due to a transposable element insertion. It was isolated in single P-element mutagenesis screen (YUE and SPRADLING 1992). Our experiments were carried out with 6 days pre-culture to deplete maternal contribution (SÁNCHEZ-SORIANO *et al.* 2010).
The *α-Spectrin* allele ***α-Spec*^{rg41}** is a protein null allele caused by a 20 bp deletion, resulting in a premature amber stop codon near the 5' end of the coding region (LEE *et al.* 1993). Our staining with anti-α-Spectrin antibody failed to detect any signal in ***α-Spec*^{rg41}** mutant primary neurons (data not shown) (HÜLSMEIER *et al.* 2007).
The *β-Spectrin* allele ***β-Spec*^{S012}** is a protein null allele caused by nucleotide substitution C538T with reference to the 2291aa isoform (HÜLSMEIER *et al.* 2007). Hemizygous *β-Spec*^{S012} mutant embryos lack detectable β-Spectrin expression (HÜLSMEIER *et al.* 2007).
The *ankyrin2* null mutant allele ***ank2*^{518}** is a transposon insertion in the 6th intron of the *ank2* gene causing the disruption of all three Ank2 isoforms (PIELAGE *et al.* 2008).
SCAR (homologue of human WASF1-3) and HEM-protein/Kette (homologue of human NCKAP1/NAP1) are essential components of the WAVE/SCAR complex required for Arp2/3-mediated nucleation in *Drosophila* neurons (SCHENCK *et al.* 2004). The mutant allele ***Hem*^{03335}** is a protein null caused by a P-element insertion 39bp downstream of the putative transcription start site (BAUMGARTNER *et al.* 1995; SCHENCK *et al.* 2004). The ***SCAR*^{Δ37}** deletion is a protein null allele caused by imprecise P-element excision (SCHENCK *et al.* 2004; ZALLEN *et al.* 2002).
Arpc1/Sop2 is the homologue of the essential regulatory Arp2/3 subunit ARPC1B/p41. The mutant ***Arpc1*^{1}** (= *Sop2*^{1}; from B. Baum) allele is caused by a 207bp genomic deletion that removes the last 62 codons of *arpc1* (HUDSON and COOLEY 2002).
***DAAM*^{Ex68}** is a null allele generated via imprecise P-element excision resulting in deletion of the C-terminal 457 amino acids, including sequences corresponding to the 'DAD' domain and most of the 'FH2' domain (MATUSEK *et al.* 2006).
The *enabled* mutant allele ***ena*^{23}** is caused by a nucleotide exchange introducing a STOP codon leading to a 52aa C-terminal truncation that deletes the EVH2 domain required for tetramerisation of Ena (AHERN-DJAMALI *et al.* 1998). In *ena*^{23} mutant embryos, anti-Ena staining (clone 5G2, mouse) is strongly reduced in primary neurons, CNSs and tendon cells (ALVES-SILVA *et al.* 2008; GONÇALVES-PIMENTEL *et al.* 2011; SÁNCHEZ-SORIANO *et al.* 2010).
The *chickadee*/profilin mutant null allele ***chic*^{221}** is caused by an intragenic deletion removing 5' non-coding and some of coding region of *chic* (VERHEYEN and COOLEY 1994; WILLS *et al.* 1999); anti-Chic staining (mouse, clone chi1J) is strongly reduced in *chic*^{221} mutant CNS and primary neurons (GONÇALVES-PIMENTEL *et al.* 2011).
The two chemically induced *short stop* mutant alleles ***shot*^{3}** and ***shot*^{sf20}** are widely used and the strongest available (likely null) alleles (KOLODZIEJ *et al.* 1995; PROKOP *et al.* 1998).
For live imaging with the ***UAS-eb1-GFP*** line (courtesy of P. Kolodziej) (SÁNCHEZ-SORIANO *et al.* 2010) we either used the pan-neuronal driver line ***sca-Gal4*** driver line for experiments at 6-8HIV (SÁNCHEZ-SORIANO *et al.* 2010), and for experiments >1DIV we used the ***elav-Gal4*^{C155}** (1st chromosome) or ***elav-Gal4*** (3rd chromosome) driver lines (LUO *et al.* 1994).
Green balancers used were *Kr::GFP* (CASSO *et al.* 2000) and *twi::GFP* (HALFON *et al.* 2002).

Cell culture

Primary neuron cultures were generated following procedures that were described in detail in previous papers (BEAVEN *et al.* 2015; PROKOP *et al.* 2012; SÁNCHEZ-SORIANO *et al.* 2010). In brief, embryos were dechorionated using bleach, selected for the correct genotypes at about stage 11 using fluorescent balancer chromosomes (stages according to Campos-

Ortega and Hartenstein) (CAMPOS-ORTEGA and HARTENSTEIN 1997), sterilised with ethanol, they were mechanically crushed and cells chemically dispersed. Cells were washed in Schneider's medium. They were either directly plated, or kept in centrifuge tubes for 3-7 days before plating in order to deplete maternal protein product (pre-culture). In both cases, cells were plated at standard concentration onto glass coverslips which were either uncoated or coated with Concanavalin A. Coverslips were kept on special incubation chambers where cells were grown as hanging drop cultures at 26ºC. For analyses at the growth cone stage, cells were grown for 6-8HIV (hours *in vitro*) on glass or ConA which were extended to 20HIV for pre-cultured neurons (always on ConA). Mature neurons were analysed at 3-10 days (always on ConA). To deplete maternal gene product, cells were pre-cultured in Schneider's medium in centrifuge tubes for up to 7 days before they were plated out as described above. For drug treatments, solutions were prepared in a cell culture medium from stock solutions in DMSO. Cells were treated with 200nM Latrunculin A (Biomol International) for 1HIV or 4HIV, 800nM or 1.6 µM Cytochalasin D (Sigma) for 1HIV or 4HIV, 20 µM nocodazole (Sigma) for 2.5HIV, or 10µM SMIFH2 (Sigma) for 4HIV, respectively. For controls, equivalent concentrations of DMSO were diluted in Schneider's medium.

Immunohistochemistry

Primary fly neurons were fixed in 4% paraformaldehyde (PFA) in 0.1 M PBS (pH 6.8 or 7.2) for 30 min at room temperature (RT), then washed three times in PBS with 0.3% TritonX-100 (PBT), followed by staining.

Antibody and actin staining and washes were performed in PBT using anti-tubulin (clone DM1A, mouse, 1:1000, Sigma; alternatively, clone YL1/2, rat, 1:500, Millipore Bioscience Research Reagents), anti-elav (clone 7E8A10, rat, 1:1000, DSHB); FITC-, Cy3- or Cy5-conjugated secondary antibodies (donkey, purified, 1:200; Jackson Immuno Research), TRITC/Alexa647-, FITC-conjugated phalloidin (1:200; Invitrogen and Sigma). Specimens were embedded in Vectashield.

For stimulated emission depletion (STED) and structured illumination microscopy (SIM), cells were cultured for 8HIV or up to 10DIV (days in vitro) at 26°C on ConA-coated 35 mm glass-bottom MatTek dishes (P35G-0.170-14-C). Cells were fixed with 4% PFA, washed 3 times in PBT, then stored for transport in PBS sealed with Parafilm. Before imaging, cells were incubated for 1hr with 2µM SiR-actin in PBS (Spirochrome) (LUKINAVIČIUS *et al.* 2014), then washed once with PBS.

Microscopy

Standard images were taken with a 100×/1.30 oil iris Ph3 ∞/0.17 objective (plus 1.6× Optovar) on an Olympus BX50WI microscope with filter sets suitable for FITC, Cy3 and Cy5 and equipped with a AxioCam camera (Zeiss). 2012 software (blue edition, Zeiss) was used to acquire images.

Time lapse live imaging of Eb1::GFP-expressing cultured neurons was performed on standard ConA-coated cover slips under temperature-controlled conditions (26°C) on a Delta Vision RT (Applied Precision) restoration microscope with a 100×/1.3 Ph3 Uplan Fl phase objective, Sedat filter set (Chroma 89000), and a Coolsnap HQ (Photometrics) camera. Images were taken every 4s for 2-3mins with exposure times of 0.5-1s, and were constructed to movies automatically.

To observe the impact of CytoD treatment on axon retraction, Eb1::GFP expressing primary neurons were cultured on 35mm glass-bottom MatTek dishes. About 10 cells per slide were filmed one-by-one for 2 mins before 800nM or 1.6 µM CytoD was applied, and then revisited for further imaging at 0hr, 0.5HIV, 1hr, 1.5HIV and 2HIV after application.

SIM was performed with an Elyra PS1 microscope (Zeiss) with a 100× oil immersion objective lens (NA = 1.46) and 642nm diode laser. Raw images were acquired with three or five grating angles. STED was performed using a Leica SP8 gated STED microscope with a 100× oil immersion objective lens (NA = 1.40), 640 nm excitation and 775 nm depletion.

Data analysis

GraphPad Prism 5 was used to calculate the mean and standard errors of the mean (SEM), and to perform statistical tests using either the Mann-Whitney U test or the Chi² test.
Filopodial lengths were measured using the segmented line tool in ImageJ. We included filopodia along axon shafts and at growth cones, but excluded those on cell bodies.
MT disorganisation was assessed as MT disorganisation index (MDI). For this, the area of disorganisation was measured using freehand selection in ImageJ. This value was then divided by axon length (measured using the segmented line tool in ImageJ) multiplied by 0.5µm (typical axon diameter), i.e. approximating axon area without disorganisation.
The relative abundance of periodic axonal actin structures (PAAS) was assessed on random SIM images of SiR-actin-stained primary neuronal cultures. On each image all identifiable axon sections of about 5um were analysed for presence of PAAS. To avoid bias, image analyses were performed blindly.
To assess frequencies of neurons with axons (Fig.3), we double-labelled primary neurons for tubulin and the neuron-specific nuclear protein Elav (ROBINOW and WHITE 1991). When defining an axon as a tubulin-stained process longer than the diameter of the soma (GONÇALVES-PIMENTEL *et al.* 2011), 76% of Elav-positive neurons display an axon in wildtype control cultures.
To assess frequencies of gaps in axons, relative numbers of primary neurons were counted where anti-tubulin along axons was discontinuous, i.e. displaying gaps (Fig.3) (ALVES-SILVA *et al.* 2012).
EB1::GFP live analyses upon actin drug treatments were performed as described previously (ALVES-SILVA *et al.* 2012). To measure speed, EB1 comets were tracked manually using the "manual tracking" plug-in of ImageJ. To analyse the number of comets, EB1 spots within an axon region of interest were counted over the whole captured time period at each of the different time points (i.e. 5, 30, 60, 90 and 120 mins after drug application), and the means of these comet numbers per axon region and time point were normalised to the mean of comet numbers in this same region before drug treatment. For each time point and treatment 6-14 different axons were analysed. Error bars shown graphs (Fig.6C-H) indicate SEM of normalised data of all axons for each time point.

To generate the autocorrelation curve (Fig.1E), images of typical axon region were intensified using ImageJ, then the data points was calculated using Mathematica 10.2. The autocorrelation function at a lag of T for an equally spaced n-point data series x_1 is given by

$$\frac{\sum_{i=1}^{n-\tau}(x_i-\bar{x})(x_{i+\tau}-\bar{x})}{\sum_{i=1}^{n}(x_i-\bar{x})^2}$$

Acknowledgement

This work was made possible through funding by the BBSRC (BB/L000717/1, BB/M007553/1) to A.P, as well as support by parents and Manchester's Faculty of Life Science to Y.Q. Microscopes at the Bioimaging Facility in Manchester were purchased with grants from BBSRC, The Wellcome Trust and the University of Manchester Strategic Fund, and the Fly Facility has been supported by funds from The University of Manchester and the Wellcome Trust (087742/Z/08/Z). Structured illumination and STED microscopes at the Research Complex at Harwell were funded by the MRC (MR/K015591/1) and BBSRC(BB/L014327/1) and imaging time was made possible through three successive grants by the STFC to A.P. We thank Simon Pearce for his support with statistical analysis, Christopher Tynan for his support with STED imaging, Andre Voelzmann and Natalia Sánchez-Soriano for helpful comments on the manuscript, and many colleagues and the Bloomington *Drosophila* Stock Center (NIH P40OD018537) for kindly providing stocks and materials (details in Suppl. Methods).

References

ADALBERT, R., and M. P. COLEMAN, 2012 Axon pathology in age-related neurodegenerative disorders. Neuropathol Appl Neurobiol **39:** 90–108.

AHERN-DJAMALI, S. M., A. R. COMER, C. BACHMANN, A. S. KASTENMEIER, S. K. REDDY *et al.*, 1998 Mutations in *Drosophila enabled* and rescue by human vasodilator-stimulated phosphoprotein (VASP) indicate important functional roles for Ena/VASP homology domain 1 (EVH1) and EVH2 domains. Mol Biol Cell **9:** 2157-2171.

ALVES-SILVA, J., I. HAHN, O. HUBER, M. MENDE, A. REISSAUS *et al.*, 2008 Prominent actin fibre arrays in *Drosophila* tendon cells represent architectural elements different from stress fibres. Mol. Biol. Cell **19:** 4287-4297.

ALVES-SILVA, J., N. SÁNCHEZ-SORIANO, R. BEAVEN, M. KLEIN, J. PARKIN *et al.*, 2012 Spectraplakins promote microtubule-mediated axonal growth by functioning as structural microtubule-associated proteins and EB1-dependent +TIPs (Tip Interacting Proteins). J. Neurosci **32:** 9143-9158.

BAINES, A. J., 2010 The spectrin-ankyrin-4.1-adducin membrane skeleton: adapting eukaryotic cells to the demands of animal life. Protoplasma **244:** 99-131.

BAUMGARTNER, S., D. MARTIN, R. CHIQUET-EHRISMANN, J. SUTTON, A. DESAI *et al.*, 1995 The HEM proteins: A novel family of tissue-specific transmembrane proteins expressed from invertebrates through mammals with an essential function in oogenesis. J Mol Biol **251:** 41-49.

BEAR, J. E., and F. B. GERTLER, 2009 ENA/VASP: towards resolving a pointed controversy at the barbed end. J. Cell Sci. **122:** 1947-1953.

BEAVEN, R., N. S. DZHINDZHEV, Y. QU, I. HAHN, F. DAJAS-BAILADOR *et al.*, 2015 *Drosophila* CLIP-190 and mammalian CLIP-170 display reduced microtubule plus end association in the nervous system. Mol Biol Cell **26:** 1491-1508.

BRADKE, F., J. W. FAWCETT and M. E. SPIRA, 2012 Assembly of a new growth cone after axotomy: the precursor to axon regeneration. Nat Rev Neurosci **13:** 183-193.

CAMPOS-ORTEGA, J. A., and V. HARTENSTEIN, 1997 *The embryonic development of Drosophila melanogaster*. Springer Verlag, Berlin.

CASSO, D., F. RAMIREZ-WEBER and T. B. KORNBERG, 2000 GFP-tagged balancer chromosomes for *Drosophila melanogaster*. Mech Dev **91:** 451-454.

D'ESTE, E., D. KAMIN, F. GÖTTFERT, A. EL-HADY and STEFAN W. HELL, 2015 STED nanoscopy reveals the ubiquity of subcortical cytoskeleton periodicity in living neurons. Cell Reports **10:** 1246-1251.

FLYNN, K. C., C. W. PAK, A. E. SHAW, F. BRADKE and J. R. BAMBURG, 2009 Growth cone-like waves transport actin and promote axonogenesis and neurite branching. Dev Neurobiol **69:** 761-779.

GALIANO, M. R., S. JHA, T. S. HO, C. ZHANG, Y. OGAWA *et al.*, 2012 A distal axonal cytoskeleton forms an intra-axonal boundary that controls axon initial segment assembly. Cell **149:** 1125-1139.

GANGULY, A., Y. TANG, L. WANG, K. LADT, J. LOI *et al.*, 2015 A dynamic formin-dependent deep F-actin network in axons. J Cell Biol.

GONÇALVES-PIMENTEL, C., R. GOMBOS, J. MIHÁLY, N. SÁNCHEZ-SORIANO and A. PROKOP, 2011 Dissecting regulatory networks of filopodia formation in a *Drosophila* growth cone model. PLoS ONE **6:** e18340.

HALFON, M. S., S. GISSELBRECHT, J. LU, B. ESTRADA, H. KESHISHIAN *et al.*, 2002 New fluorescent protein reporters for use with the *Drosophila* Gal4 expression system and for vital detection of balancer chromosomes. Genesis **34:** 135-138.

HAMMARLUND, M., E. M. JORGENSEN and M. J. BASTIANI, 2007 Axons break in animals lacking beta-spectrin. J Cell Biol **176:** 269-275.

HANNEZO, E., B. DONG, P. RECHO, J. F. JOANNY and S. HAYASHI, 2015 Cortical instability drives periodic supracellular actin pattern formation in epithelial tubes. Proc Natl Acad Sci U S A.

HUDSON, A. M., and L. COOLEY, 2002 A subset of dynamic actin rearrangements in *Drosophila* requires the Arp2/3 complex. J Cell Biol **156:** 677-687.

HÜLSMEIER, J., J. PIELAGE, C. RICKERT, G. M. TECHNAU, C. KLÄMBT *et al.*, 2007 Distinct functions of {alpha}-Spectrin and {beta}-Spectrin during axonal pathfinding. Development **134:** 713-722.

KA, M., E. M. JUNG, U. MUELLER and W. Y. KIM, 2014 MACF1 regulates the migration of pyramidal neurons via microtubule dynamics and GSK-3 signaling. Dev Biol **395:** 4-18.

KALIL, K., and E. W. DENT, 2014 Branch management: mechanisms of axon branching in the developing vertebrate CNS. Nat Rev Neurosci **15:** 7-18.

KAPUR, M., W. WANG, M. T. MALONEY, I. MILLAN, V. F. LUNDIN *et al.*, 2012 Calcium tips the balance: a microtubule plus end to lattice binding switch operates in the carboxyl terminus of BPAG1n4. EMBO Rep **13:** 1021-1029.

KOLODZIEJ, P. A., L. Y. JAN and Y. N. JAN, 1995 Mutations that affect the length, fasciculation, or ventral orientation of specific sensory axons in the *Drosophila* embryo. Neuron **15:** 273-286.

KRUER, M. C., T. JEPPERSON, S. DUTTA, R. D. STEINER, E. COTTENIE *et al.*, 2013 Mutations in gamma adducin are associated with inherited cerebral palsy. Annals of Neurology **74:** 805-814.

KÜPPERS-MUNTHER, B., J. LETZKUS, K. LÜER, G. TECHNAU, H. SCHMIDT *et al.*, 2004 A new culturing strategy optimises *Drosophila* primary cell cultures for structural and functional analyses. Dev. Biol. **269:** 459-478.

LEE, J. K., R. S. COYNE, R. R. DUBREUIL, L. S. GOLDSTEIN and D. BRANTON, 1993 Cell shape and interaction defects in alpha-spectrin mutants of *Drosophila melanogaster*. J Cell Biol **123:** 1797-1809.

LI, X., Y. KUMAR, H. ZEMPEL, E. M. MANDELKOW, J. BIERNAT *et al.*, 2011 Novel diffusion barrier for axonal retention of Tau in neurons and its failure in neurodegeneration. EMBO J **30:** 4825-4837.

LORENZO, D. N., M. G. LI, S. E. MISCHE, K. R. ARMBRUST, L. P. RANUM *et al.*, 2010 Spectrin mutations that cause spinocerebellar ataxia type 5 impair axonal transport and induce neurodegeneration in *Drosophila*. J Cell Biol **189:** 143-158.

LUKINAVIČIUS, G., L. REYMOND, E. D'ESTE, A. MASHARINA, F. GÖTTFERT *et al.*, 2014 Fluorogenic probes for live-cell imaging of the cytoskeleton. Nature Methods **11:** 731-733.

LUO, L., Y. J. LIAO, L. Y. JAN and Y. N. JAN, 1994 Distinct morphogenetic functions of similar small GTPases: *Drosophila* Drac1 is involved in axonal outgrowth and myoblast fusion. Genes Dev. **8:** 1787-1802.

MACHNICKA, B., A. CZOGALLA, A. HRYNIEWICZ-JANKOWSKA, D. M. BOGUSLAWSKA, R. GROCHOWALSKA *et al.*, 2014 Spectrins: a structural platform for stabilization and activation of membrane channels, receptors and transporters. Biochim Biophys Acta **1838:** 620-634.

MATUSEK, T., A. DJIANE, F. JANKOVICS, D. BRUNNER, M. MLODZIK *et al.*, 2006 The *Drosophila* formin DAAM regulates the tracheal cuticle pattern through organizing the actin cytoskeleton. Development **133:** 957-966.

MYERS, K. A., Y. HE, T. P. HASAKA and P. W. BAAS, 2006 Microtubule transport in the axon: Re-thinking a potential role for the actin cytoskeleton. Neuroscientist **12:** 107-118.

PETERSON, J. R., and T. J. MITCHISON, 2002 Small molecules, big impact: a history of chemical inhibitors and the cytoskeleton. Chem Biol **9:** 1275-1285.

PIELAGE, J., L. CHENG, R. D. FETTER, P. M. CARLTON, J. W. SEDAT *et al.*, 2008 A presynaptic giant ankyrin stabilizes the NMJ through regulation of presynaptic microtubules and transsynaptic cell adhesion. Neuron **58:** 195-209.

PROKOP, A., 2013 The intricate relationship between microtubules and their associated motor proteins during axon growth and maintenance. Neur Dev **8:** 17.

PROKOP, A., R. BEAVEN, Y. QU and N. SÁNCHEZ-SORIANO, 2013 Using fly genetics to dissect the cytoskeletal machinery of neurons during axonal growth and maintenance. J. Cell Sci. **126:** 2331-2341.

PROKOP, A., B. KÜPPERS-MUNTHER and N. SÁNCHEZ-SORIANO, 2012 Using primary neuron cultures of *Drosophila* to analyse neuronal circuit formation and function, pp. 225-247 in *The making and un-making of neuronal circuits in Drosophila*, edited by B. A. HASSAN. Humana Press, New York.

PROKOP, A., J. UHLER, J. ROOTE and M. C. BATE, 1998 The *kakapo* mutation affects terminal arborisation and central dendritic sprouting of *Drosophila* motorneurons. J. Cell Biol. **143:** 1283-1294.

RASBAND, M. N., 2010 The axon initial segment and the maintenance of neuronal polarity. Nat Rev Neurosci **11:** 552-562.

ROBINOW, S., and K. WHITE, 1991 Characterization and spatial distribution of the Elav protein during *Drosophila melanogaster* development. J. Neurobiol. **22:** 443-461.

SÁNCHEZ-SORIANO, N., C. GONÇALVES-PIMENTEL, R. BEAVEN, U. HAESSLER, L. OFNER *et al.*, 2010 *Drosophila* growth cones: a genetically tractable platform for the analysis of axonal growth dynamics. Dev. Neurobiol. **70:** 58-71.

SÁNCHEZ-SORIANO, N., M. TRAVIS, F. DAJAS-BAILADOR, C. GONCALVES-PIMENTEL, A. J. WHITMARSH *et al.*, 2009 Mouse ACF7 and *Drosophila* Short stop modulate filopodia formation and microtubule organisation during neuronal growth. J Cell Sci **122:** 2534-2542.

SCHENCK, A., A. QURASHI, P. CARRERA, B. BARDONI, C. DIEBOLD *et al.*, 2004 WAVE/SCAR, a multifunctional complex coordinating different aspects of neuronal connectivity. Dev Biol **274:** 260-270.

SMITH, D. H., M. NONAKA, R. MILLER, M. LEONI, X. H. CHEN *et al.*, 2000 Immediate coma following inertial brain injury dependent on axonal damage in the brainstem. J Neurosurg **93:** 315-322.

VERHEYEN, E. M., and L. COOLEY, 1994 Profilin mutations disrupt multiple actin-dependent processes during *Drosophila* development. Development **120:** 717–728.

WATANABE, K., S. AL-BASSAM, Y. MIYAZAKI, T. J. WANDLESS, P. WEBSTER *et al.*, 2012 Networks of polarized actin filaments in the axon initial segment provide a mechanism for sorting axonal and dendritic proteins. Cell Rep **2:** 1546-1553.

WILLS, Z., L. MARR, K. ZINN, C. S. GOODMAN and D. VAN VACTOR, 1999 Profilin and the Abl tyrosine kinase are required for motor axon outgrowth in the *Drosophila* embryo. Neuron **22:** 291-299.

WU, X., Q. T. SHEN, D. S. ORISTIAN, C. P. LU, Q. ZHENG *et al.*, 2011 Skin stem cells orchestrate directional migration by regulating microtubule-ACF7 connections through GSK3beta. Cell **144:** 341-352.

XU, K., G. ZHONG and X. ZHUANG, 2013 Actin, Spectrin, and associated proteins form a periodic cytoskeletal structure in axons. Science **339:** 452-456.

YANG, Y., C. BAUER, G. STRASSER, R. WOLLMAN, J. P. JULIEN *et al.*, 1999 Integrators of the cytoskeleton that stabilize microtubules. Cell **98:** 229-238.

YUE, L., and A. C. SPRADLING, 1992 hu-li tai shao, a gene required for ring canal formation during *Drosophila* oogenesis, encodes a homolog of adducin. Genes Dev **6:** 2443-2454.

ZALLEN, J. A., Y. COHEN, A. M. HUDSON, L. COOLEY, E. WIESCHAUS *et al.*, 2002 SCAR is a primary regulator of Arp2/3-dependent morphological events in *Drosophila*. J Cell Biol **156:** 689-701.

ZHANG, Y., V. HA, H. LI, A. V. TZINGOUNIS and G. LYKOTRAFITIS, 2016 Axon membrane skeleton structure is optimized for coordinated sodium propagation. ArXiv**:** arXiv:1602.06348.

ZHONG, G., J. HE, R. ZHOU, D. LORENZO, H. P. BABCOCK *et al.*, 2014 Developmental mechanism of the periodic membrane skeleton in axons. Elife **3**.

Figures

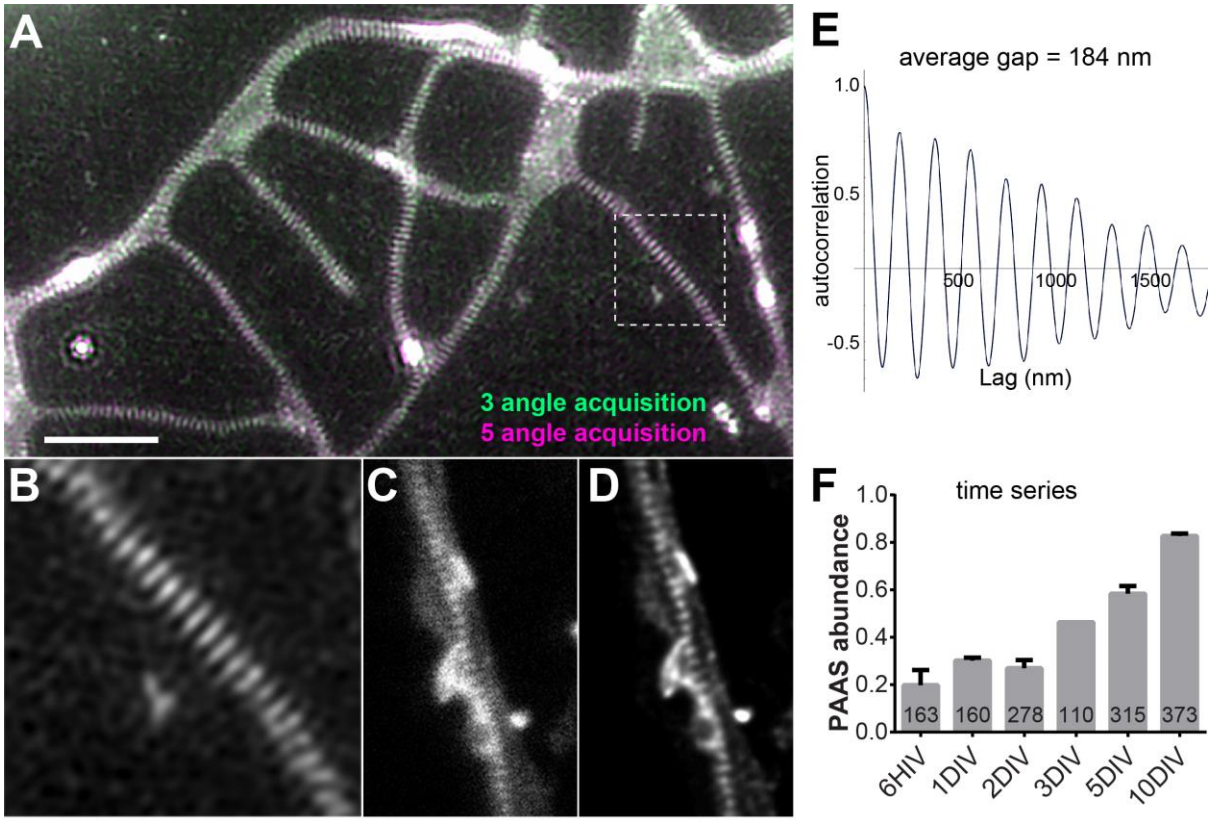

Fig.1. PAAS are conserved in fly neurons. (**A-D**) Super-resolution images of SiR-actin-stained *Drosophila* primary neurons at 10DIV, imaged with SIM (A; framed area shown magnified in B) or STED (C, raw image; D, deconvolved); the image in A shows precise overlay of two independent rounds of image acquisition using three (green) versus five (magenta) rotation angles. All images show periodic actin structures with a lag of 184nm, as determined by autocorrelation analysis (**E**). (**F**) PAAS abundance gradually increases from 6HIV to 10DIV; numbers in the bars are sample numbers (i.e. analysed regions of interest), error bars represent SEM of independent experimental repeats. Scale bar in A represents 3µm in A and 1.2µm in B–D.

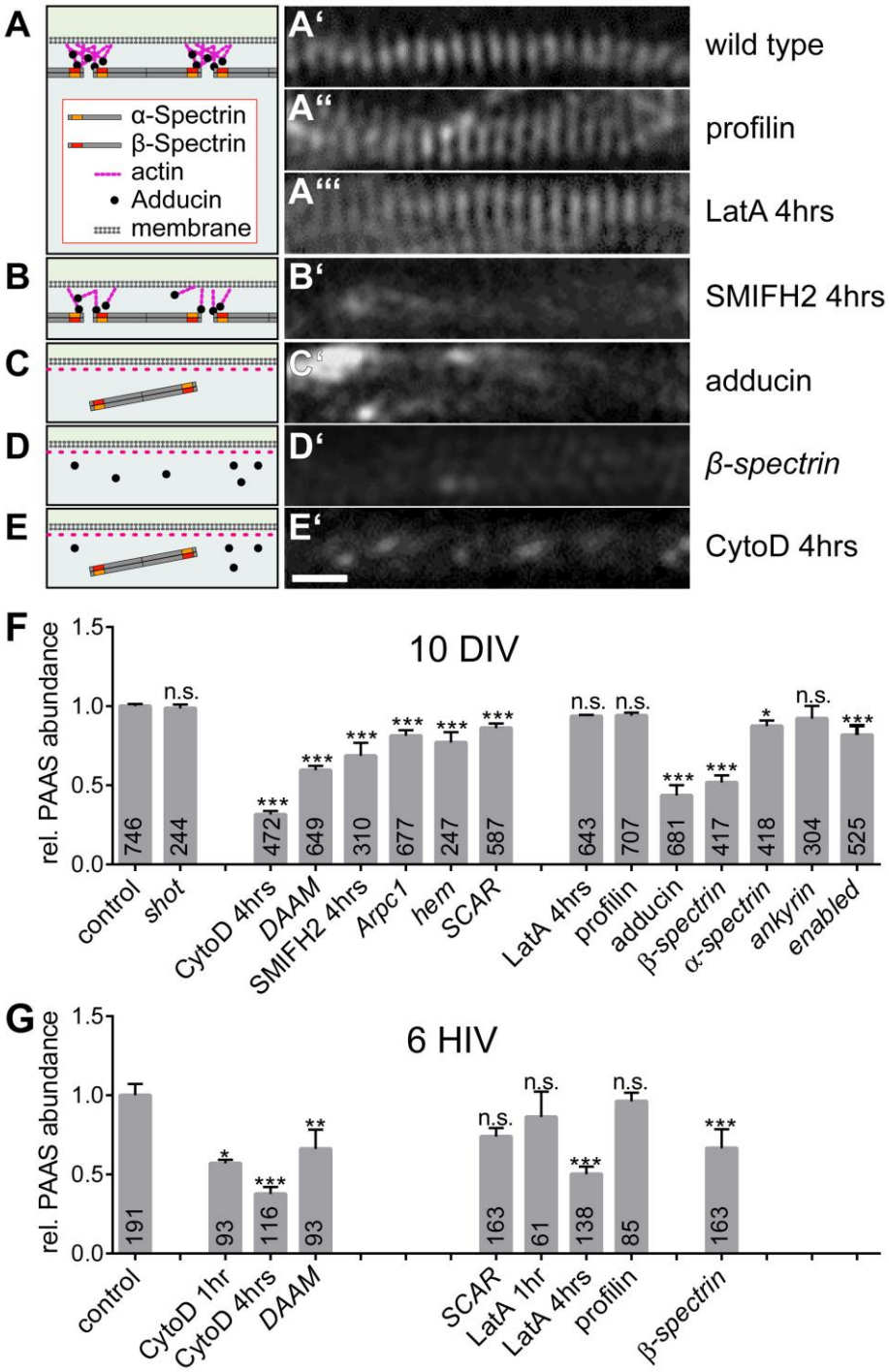

Fig.2. Functional dissection of PAAS. (**A-E**) Representative SIM images of SiRActin-labelled axons at 10DIV genetically or pharmacologically manipulated as indicated on the right; schematics on the left provide an interpretation of the observed phenotype, based on the previously proposed cortical actin model (Xu *et al.* 2013). (**F, G**) Quantification of PAAS abundance in mature (F; 10DIV) and young (G; 6HIV) neurons, given as percentage of blindly chosen ~5µm axon segments displaying periodic actin structures and normalised to controls. P values were obtained via χ^2 analysis of raw data comparing axon segments with/without PAAS (NS P>0.050,*P≤0.05; **P≤0.010; ***P≤0.001); numbers in bars represent sample numbers (i.e. analysed axon segments); error bars represent SEM of independent experimental repeats; details in Table S1. Scale bar in E'=550nm for all SIM images.

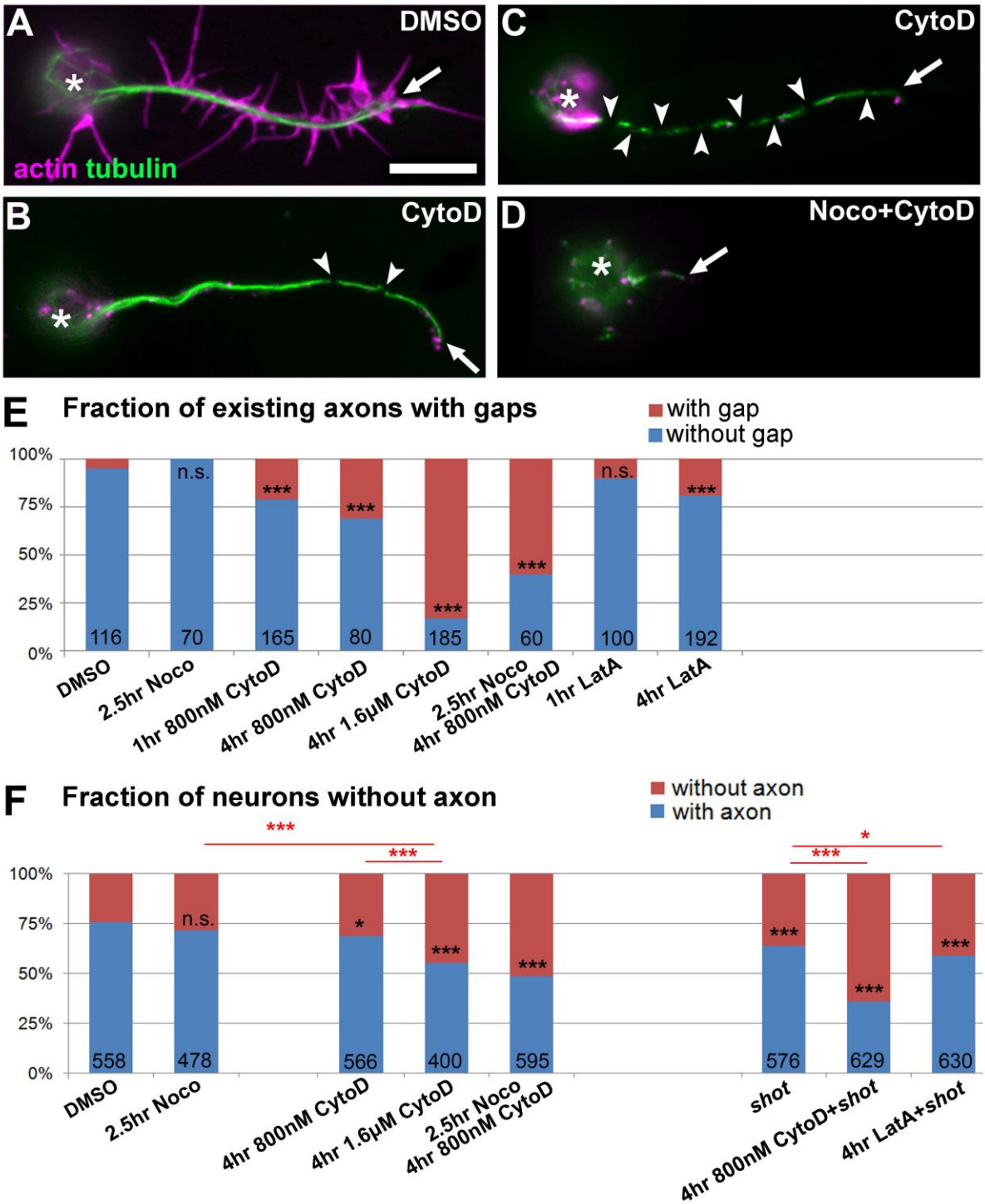

Fig.3. F-actin has MT stabilising roles. (**A-D**) Primary wildtype neurons at 8HIV stained for actin (magenta) and tubulin (green), either untreated (wt) or treated with CytoD and/or nocodazole (noco) as indicated (asterisks, cell body; arrows, axon tips; arrowheads, MT gaps); images show gap phenotypes (mild in B, strong in C) and axon loss (D). Quantification of axon gap phenotypes (**E**) and axon loss phenotypes (**F**); numbers in bars refer to analysed neurons; all data were compared to DMSO controls via χ^2 analysis (NS P>0.050, *P<0.050, **P<0.010,***P<0.001); for detailed data see Tab.S2,3. Scale bar in A represents 10µm in A-D.

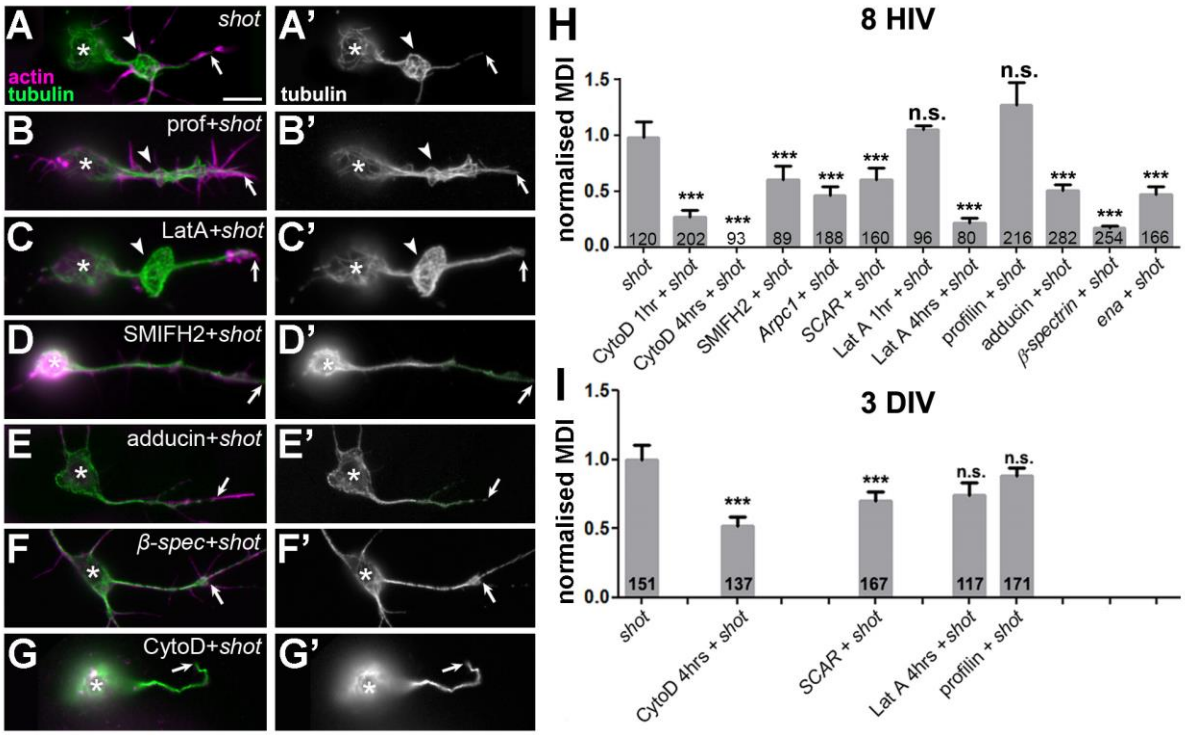

Fig.4. F-actin manipulations in *shot* mutant neurons. (**A-G'**) *shot* mutant primary neurons at 8HIV stained for tubulin (green) and actin (magenta) combined with different actin manipulation as indicated (asterisks, cell bodies; arrows, axon tips; arrowheads, areas of MT disorganisation). Quantifications of MDI for neurons at 8HIV (**H**) and 3DIV (**I**); numbers in bars refer to neurons analysed; all data normalised to *shot;* for detailed data see Tab.S4. P values were calculated using the Mann-Whitney Rank Sum test (NS P>0.050, *P<0.050, **P<0.010, ***P<0.001). Scale bar in A represents 10μm in A-G'.

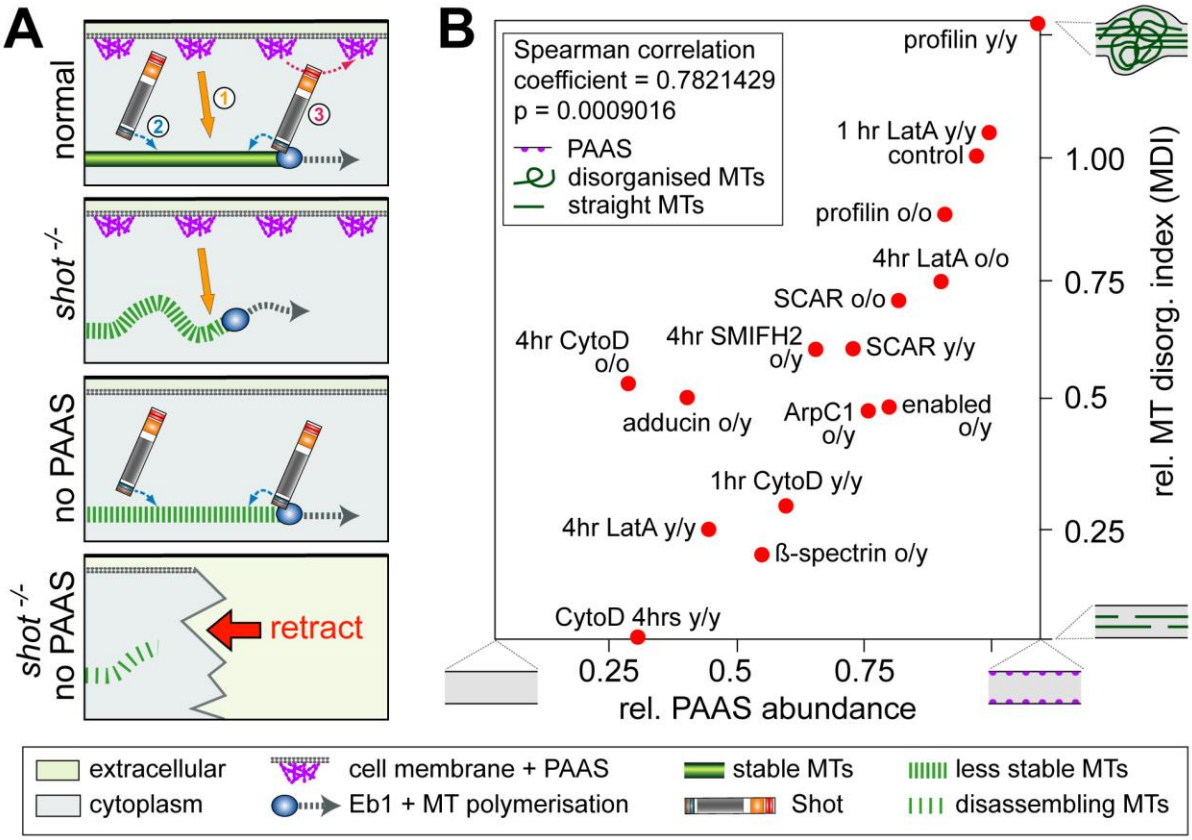

Fig.5. Presence of cortical actin correlates with MDI values. (**A**) Schematics illustrating roles of actin in MT stabilisation (1; orange arrow; this paper) and two independent roles of Shot in maintaining coalescent MT bundles: through MT/MT bundle stabilisation (2; blue arrow) and guidance of polymerising MTs into parallel bundles (3) (ALVES-SILVA *et al.* 2012); upon Shot deficiency MTs become less stable and disorganised, upon PAAS loss MTs become less stable, loss of both leads to MT disassembly and axon retraction (symbols explained in box below). (**B**) Correlation plot comparing degrees of PAAS abundance (data from Fig.2) with degrees of MDI (data from Fig.4); in each pairing "o" indicates old neurons (3 or 10DIV) and "y" young neurons (6-8HIV) with regard to PAAS analysis (before slash) and MDI analysis (after slash); extreme phenotypes for PAAS abundance and MDI are symbolised as explained in inset. See Fig.S3 for further explanations.

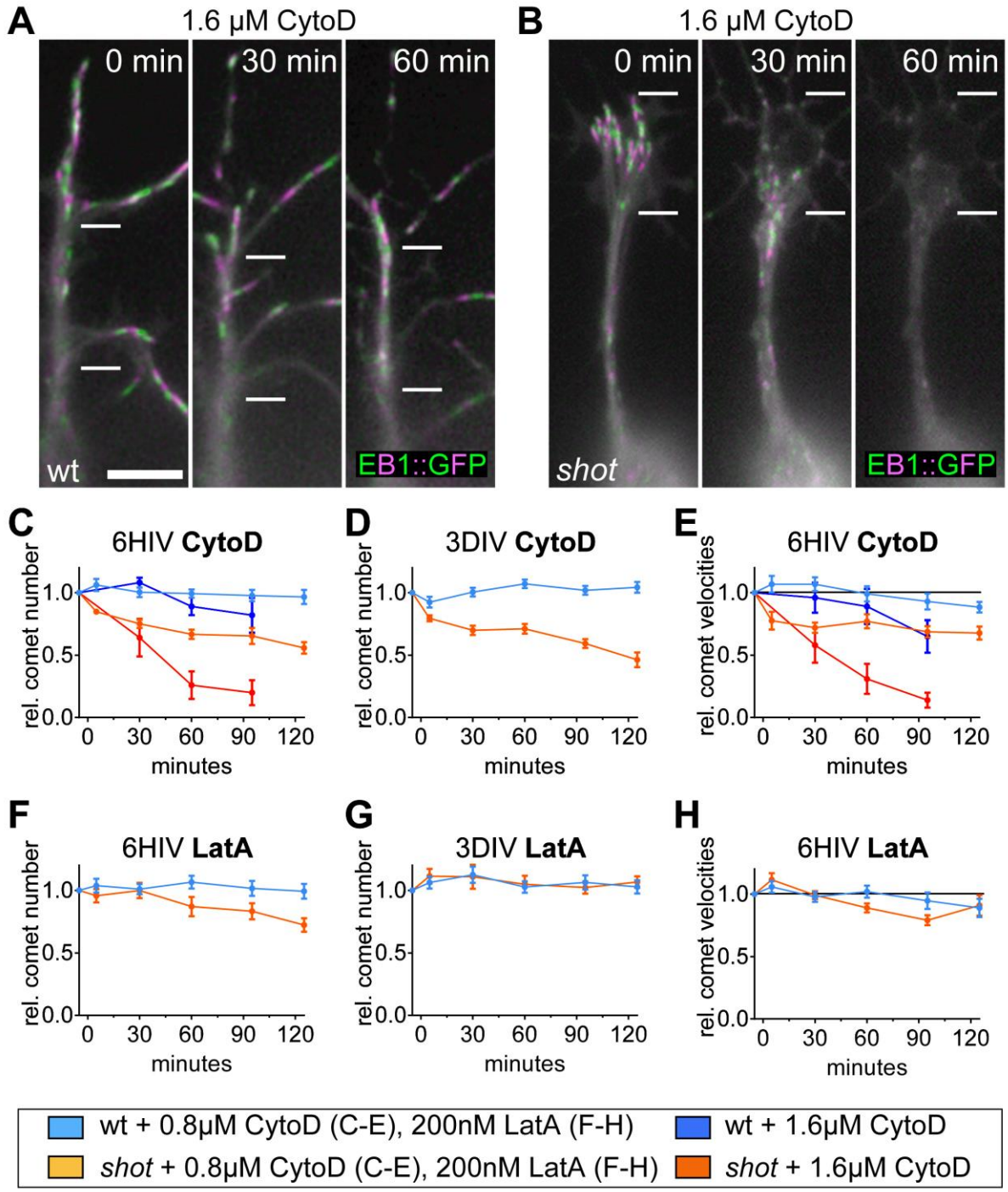

Fig.6. Live recordings of wildtype and *shot* deficient primary neurons expressing EB1::GFP. (A, B) Stills of movies of neurons at 6HIV taken at three time points (0, 30 and 60 min after treatment), where each still is a projection of four images which are 3s apart and alternatingly coloured in green and magenta to indicate the movement of EB1::GFP comets; note that comets come to a hold and vanish only in *shot* mutant neurons. Measurements of comet numbers (C, D, F, G) and velocities (E, H) of EB1::GFP comets in wild-type and *shot*[3] mutant neurons upon treatment with either 0.8µM CytoD, 1.6µM CytoD or 200nM LatA respectively, as indicated in box below; velocity of WT is 0.154µm/s ± 0.01SEM; details in Tab.S5. Scale bar indicates 5µm.